Urbani, S., Acocella, V., Rivalta, E., Corbi, F. (2017): Propagation and arrest of dikes under topography: models applied to the 2014 Bardarbunga (Iceland) rifting event. - *Geophysical Research Letters*, *44*, 13, pp. 6692—6701.

DOI: http://doi.org/10.1002/2017GL073130

AGU PUBLICATIONS

Geophysical Research Letters

RESEARCH LETTER
10.1002/2017GL073130

Key Points:
- Recent diking events along rift zones showed that dikes can propagate laterally for tens of kilometers arresting before reliefs
- Analogue models show that topographic lateral pressure gradient and crustal rigidity layering assist lateral propagation
- Numerical models show that the stress field induced by topography leads to dike arrest

Supporting Information:
- Supporting Information S1
- Figure S1
- Figure S2
- Figure S3

Correspondence to:
S. Urbani,
stefano.urbani@uniroma3.it

Citation:
Urbani, S., V. Acocella, E. Rivalta, and F. Corbi (2017), Propagation and arrest of dikes under topography: Models applied to the 2014 Bardarbunga (Iceland) rifting event, *Geophys. Res. Lett.*, *44*, 6692–6701, doi:10.1002/2017GL073130.

Received 17 FEB 2017
Accepted 18 JUN 2017
Accepted article online 20 JUN 2017
Published online 7 JUL 2017

Propagation and arrest of dikes under topography: Models applied to the 2014 Bardarbunga (Iceland) rifting event

S. Urbani[1], V. Acocella[1], E. Rivalta[2], and F. Corbi[3]

[1]Dipartimento di Scienze, Università Roma Tre, Rome, Italy, [2]Deutsches GeoForschungsZentrum GFZ, Potsdam, Germany, [3]Géosciences Montpellier Laboratory, University of Montpellier, Montpellier, France

Abstract Dikes along rift zones propagate laterally downslope for tens of kilometers, often becoming arrested before topographic reliefs. We use analogue and numerical models to test the conditions controlling the lateral propagation and arrest of dikes, exploring the presence of a slope in connection with buoyancy and rigidity layering. A gentle downslope assists lateral propagation when combined with an effective barrier to magma ascent, e.g., gelatin stiffness contrasts, while antibuoyancy alone may be insufficient to prevent upward propagation. We also observe that experimental dikes become arrested when reaching a plain before opposite reliefs. Our numerical models show that below the plain the stress field induced by topography hinders further dike propagation. We suggest that lateral dike propagation requires an efficient barrier (rigidity) to upward propagation, assisting antibuoyancy, and a lateral pressure gradient perpendicular to the least compressive stress axis, while dike arrest may be induced by external reliefs.

1. Introduction

Recent diking events suggest that topography plays a role in both driving and arresting lateral dike propagation. For example, the 2014 Bardarbunga (Iceland) dike propagated for tens of kilometers downslope before arresting below a plain in front of the Askja volcanic edifice [*Sigmundsson et al.*, 2015]. At the volcanic edifice scale, feeder dikes have also propagated downslope and arrested before opposite reliefs, as on Somma-Vesuvio, Italy [*Acocella et al.*, 2006]. The lateral propagation of magma has been commonly attributed to density contrasts with the host rock, with the magma reaching the level of neutral buoyancy [*Lister*, 1990, 1991; *Lister and Kerr*, 1991; *Ryan*, 1994; *Rubin*, 1995, and references therein; *Taisne and Jaupart*, 2009]. A lateral stress gradient, of tectonic [*Dahm et al.*, 2010], rheological [*Grandin et al.*, 2012], or topographic [e.g., *Fialko and Rubin*, 1999; *Buck et al.*, 2006] origin, may be also necessary to drive dikes laterally. Since many dikes originate from magma chambers below volcanic edifices, the role played by topographic stresses in driving dike propagation and facilitating arrest may often dominate [*Fiske and Jackson*, 1972; *Pinel and Jaupart*, 2000, 2004, 2005; *Watanabe et al.*, 2002; *Acocella and Tibaldi*, 2005; *Acocella et al.*, 2006; *Kervyn et al.*, 2009; *Roman and Jaupart*, 2014; *Maccaferri et al.*, 2016].

Other factors may discourage magma ascent, indirectly favoring lateral dike propagation. These include dike-induced graben faulting [*Xu et al.*, 2016] and layering [*Gudmundsson*, 2002, 2011; *Maccaferri et al.*, 2011], or a stiffer upper layer [*Rivalta et al.*, 2005; *Kavanagh et al.*, 2006; *Ritter et al.*, 2013]. A weak upper layer may also arrest dike ascent, as not storing much stress [*Gudmundsson*, 2003]. These studies considered only the role of a single feature in lateral dike propagation. Here we use experiments to investigate the joint role of topography, layering, and density on lateral dike propagation and arrest; we present a representative selection of our data set of 20 experiments (Table S1 in the supporting information). We complement these with numerical models describing quantitatively the stress field affecting the experiments.

2. Experimental Setup and Scaling

We injected dyed water in a $33 \times 58 \times 38.5$ cm^3 plexiglass box filled with pig-skin gelatin [*Di Giuseppe et al.*, 2009] as magma and upper crust analogues, respectively (Figure 1a). In each experiment we imposed a layering using two concentrations of gelatin and/or adding NaCl (2.5–4 wt % and 0–10 wt %, respectively) [*Brizzi et al.*, 2016]. Similarly, we added NaCl to increase water density ($\rho_f = 1053.6$ kg m^{-3}), so that ρ_f is comprised between the density of the upper (ρ_u) and lower (ρ_l) layers (i.e., $\rho_l > \rho_f > \rho_u$), ρ_u/ρ_f being constant. We then

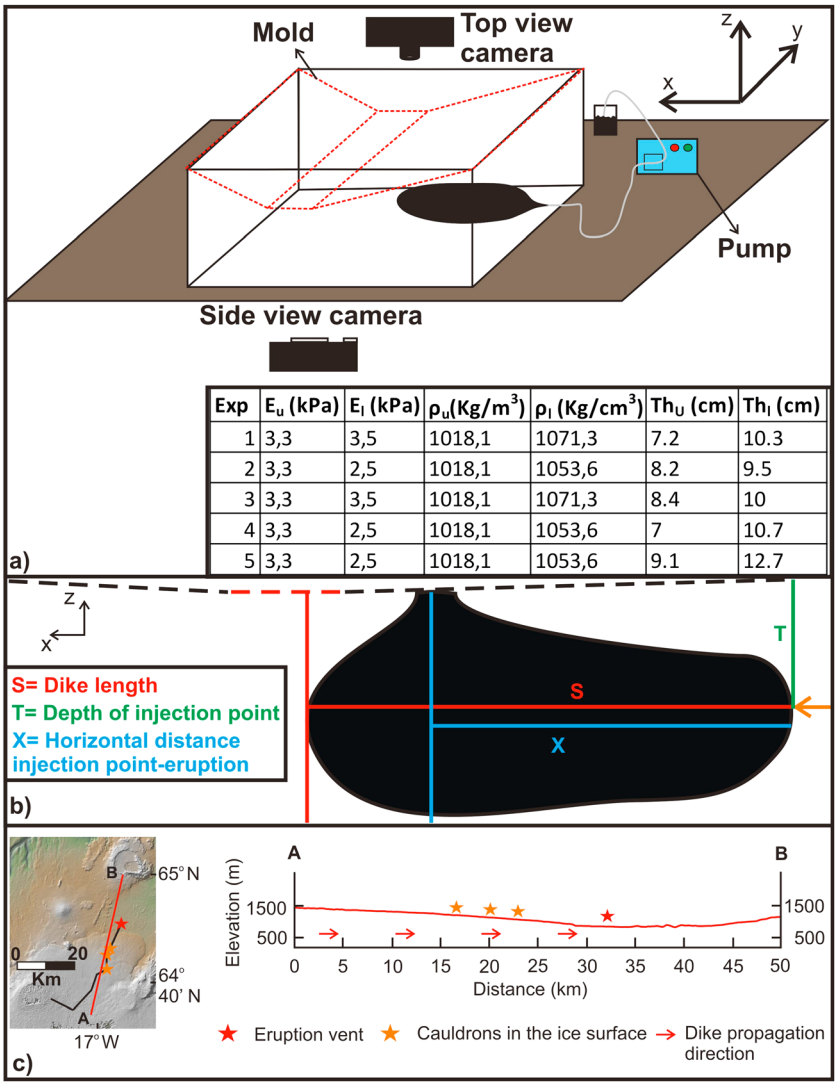

Exp	E_u (kPa)	E_l (kPa)	ρ_u(Kg/m^3)	ρ_l (Kg/cm^3)	Th_U (cm)	Th_l (cm)
1	3,3	3,5	1018,1	1071,3	7.2	10.3
2	3,3	2,5	1018,1	1053,6	8.2	9.5
3	3,3	3,5	1018,1	1071,3	8.4	10
4	3,3	2,5	1018,1	1053,6	7	10.7
5	3,3	2,5	1018,1	1053,6	9.1	12.7

Figure 1. (a) Experimental setup. The reference system in the top right refers to the box sides. Inset in the bottom right shows the values of the young modulus (E), density (ρ), and thickness (Th) of the upper (E_u, ρ_u, and Th_u) and lower layers (E_l, ρ_l, and Th_l) in the representative experiments. (b) Calculations of S, X, and T (see inset on the left) in each experiment. The dashed black and red lines indicate the slopes and the plain, respectively. The orange arrow indicates the injection point. (c) Topography profile along approximate pathway of Bardarbunga dike (elevation:distance = 1:2). The black line in map view indicates the surface projection of the dike.

poured the upper layer's solution gently on top of the bottom one while this was still liquid, so the two layers mixed partially and we obtained, after cooling, an ~4 cm thick, nonsharp interface with a concentration gradient. We refer to density layering when the two layers have the same rigidity but different densities (E_u/E_l~1, where E_u and E_l are the rigidity of the upper and lower layer, respectively) and to rigidity layering when $E_u/E_l > 1$, regardless of their densities (Table S1). We fixed the thickness ratio between the upper and lower layer as between 0.7 and 0.8. The temperatures of the gelatin and water were 9 and 20°C, respectively.

We shaped the gelatin surface using a mold with gently inward dipping flanks (2.4° and 3.7°) separated by a 8 cm wide horizontal plain (Figure 1a). This configuration allows investigating the role of two opposite slopes on dike propagation. It roughly simulates the 2-D along-strike topography of the 2014 Bardarbunga intrusion (Figure 1c), considered representative of a dike propagating laterally downslope. We avoided any local stress due to the central volcano [see *Corbi et al.*, 2015 and 2016 instead]. Hereafter we refer to "topography"

models indicating experiments having this profile. In experiment 5 (Table S1), we increased to 7° the dip of the slope, without any opposite slope. We injected dyed water from the box side using a peristaltic pump (Figure 1a) with constant influx rate of 0.079 mL/s. We held the needle tip on the *x-z* plane (Figures 1a, 1b, and 2a–2d), aiming to impose the initial dike strike parallel to the same plane.

We monitored the dike propagation in side and top view at 0.1 frames per second, measuring the final dike length and horizontal distance between the eruption and injection points (*S* and *X*, respectively; Figure 1b).

Below are the calculations to scale our models. The difference in density between gelatin and water in the models is ~20 kg m^{-3}. As for nature, we take the density difference between basaltic dikes and host rock as ~20 kg m^{-3}, with ρ_{solid} = 2800 kg m^{-3}; thus, $\Delta\rho^*$ is 1 (where asterisk refers to the ratio of the parameter values measured at the laboratory and natural scale). The fracture toughness (K_c) of the gelatin is calculated from *Kavanagh et al.* [2013]:

$$K_c = (1.4 \pm 0.1)\sqrt{E} \tag{1}$$

where the Young's modulus, *E*, is 3.5 kPa for pig-skin gelatin [*Ritter*, 2012] and K_c = 83 Pa $m^{1/2}$. K_c of natural rocks spans from 10^6 to 10^9 Pa $m^{1/2}$, based on laboratory studies or field estimates, respectively [*Scholz*, 2010; *Olson and Schultz*, 2011; *Rivalta et al*., 2015, and references therein]. We assume that K_c in nature is ~10^9 Pa $m^{1/2}$, which is appropriate for tens of kilometer-long dikes [*Rivalta et al*., 2015]; therefore, $K_c^* = 8.3 \times 10^{-8}$. The dimensionless scaling ratios between model and nature for the propagation velocity (V^*), rigidity (E^*), and buoyancy length (L_b^*) are as follows [*Kavanagh et al*., 2013]:

$$L_b^* = (K_c^*/\Delta\rho^*)^{2/3} = 1.9 \times 10^{-5} \tag{2}$$

$$V^* = (\Delta\rho^*)^{1/6}\, {K_c^*}^{1/3}\, {\rho^*_{solid}}^{-1/2} = 7.2 \times 10^{-3} \tag{3}$$

$$E^* = \Delta\rho^*\, L_b^* (L/\Psi)^* = 1.9 \times 10^{-7} \tag{4}$$

where Ψ is the dike thickness.

Therefore, the height of our dikes corresponds to ~5.8 and ~7.6 km in nature, similar to the Bardarbunga dike or the main dike of the Dabbahu (Afar, Ethiopia) sequence. The thickness of the experimental dikes (≤1 mm) corresponds to a few meters in nature [*Rivalta et al*., 2015, equation (4)].

We additionally define the time scaling factor as

$$t^* = L^*/V^* \tag{5}$$

Observed velocities of laterally propagating dikes in Iceland and Afar are ~7–112 km per day [*Wright et al*., 2012; *Ágústsdóttir et al*., 2016], thus on the upper side of our experimental ones (~6 km per day; section 3.1).

We now compare the ratio *r* between the vertical pressure gradient (buoyancy) and the horizontal pressure gradient (loading) in the model and nature:

$$r\,(\text{nature}) = (\Delta\rho\ L)/(\rho\ \Delta h) = 0.46 \tag{6}$$

where *L* = 45 km and Δh = 700 m, as in the Bardarbunga case;

$$r\,(\text{model}) = (\Delta\rho\ L)/(\rho\ \Delta h) = 0.52 \tag{7}$$

where *L* = 32 cm and Δh = 1.3 cm. Since the ratios are similar, the two gradients play a similar relative role in experiments and nature.

To scale additional pressure contributions, we need more parameters, as follows: volumetric flux into the dike (*Q*) is 7.9×10^{-8} m^3 s^{-1} in the models and 286 m^3 s^{-1} for Bardarbunga [*Gudmundsson et al*., 2016]; thus,

$Q^* = 2.76 \times 10^{-10}$. Shear modulus (μ) is 1.17×10^3 Pa in the models and 0.3×10^{11} Pa for basalts [*Turcotte and Schubert*, 2002]; thus, $\mu^* = 3.89 \times 10^{-8}$. Fluid viscosity ($\eta$) is 1.2×10^{-3} Pa s in the models and 10 Pa s for basalts; thus, $\eta^* = 1.2 \times 10^{-4}$. Poisson's ratio ($\nu$) is 0.5 for pig-skin gelatin and 0.25 in nature; thus, $(1-\nu)^* = 0.67$. We now calculate the

1. topographic (loading) pressure scale ratio:

$$p_L{}^* = (\rho^* g^* \Delta h^*) = 0.6 \times 10^{-5} \tag{8}$$

where $\rho^* = 1000$ kg m^{-3}/2800 kg m^{-3} = 0.36 and $\Delta h^* = 1.3 \times 10^{-2}$ m/700 m = 1.9×10^{-5}

2. fracture pressure scale ratio [*Rivalta et al*., 2015, equation (28)]:

$$p_f{}^* = \left(\Delta\rho^* g^* K_c{}^{*2}\right)^{1/3} = 1.9 \times 10^{-5} \tag{9}$$

3. viscous pressure scale ratio [*Rivalta et al*., 2015, equation (25)]:

$$p_v{}^* = \left(\left(\mu^{*3} Q^* \eta^* \Delta\rho^{*2}\right)/(1-\nu)^{*3}\right)^{1/6} = 1.1 \times 10^{-6} \tag{10}$$

For the range of parameters considered, while the viscous pressure drop is slightly higher in nature than experiments, we find that $p_L{}^*$ and $p_f{}^*$ are similar: this ensures, together with equations (6) and (7), that the loading gradient and fracturing play a similar proportional role in nature and experiments.

We assume that (1) there is no phase change (vesiculation or solidification) in the magma; this assumption is not excessively restrictive for the mafic lateral dike intrusions that we aim to study. (2) Steady magma inflow into the dike; in reality, inflow decreased with time changing the ratio between fracture and viscous pressure. A possible limitation is the finite size of the box and of the gelatin layers, as addressed with additional numerical models. (3) We neglect any effect of regional extension or of preexisting tectonic discontinuities.

3. Results

3.1. Experiments

We first describe two experiments with flat topography (experiments 1 and 2, respectively; Figures 2a and 2b) and then compare these with two experiments representative of the general influence of topography on dike propagation with density and rigidity layering (experiments 3 and 4 respectively; Figures 2c and 2d and Table S1). We describe the shape of the dike in each experiment (breadth/height (*B*/*H*)) to evaluate any change due to the imposed factors.

In experiment 1 (density layering; Figure 2a), the dike propagated vertically penetrating the upper medium and elongating laterally close to the surface prior to erupting after 300 s (1.3 days in nature). This resulted in final aspect ratio (*B*/*H*) and length (*S*) of 0.84 and 8.55 cm, respectively. The mean lateral and vertical propagation velocities were 0.48 and 0.61 mm/s, respectively.

In experiment 2 (rigidity layering; Figure 2b), the dike propagated laterally at the interface with the stiff upper layer, erupting after 1320 s (~6 days in nature). The final aspect ratio and length were 1.45 and 21.3 cm, respectively. The mean lateral and vertical propagation velocities were 0.28 and 0.24 mm/s, respectively.

In experiment 3 (topography and density layering; Figure 2c), the dike propagated vertically, showing a similar shape to experiment 1 and erupting after 330 s (~1.5 days in nature). The final aspect ratio and length were 0.90 and 9.1 cm, respectively. The mean lateral and vertical propagation velocities were 0.46 and 0.56 mm/s, respectively.

In experiment 4 (topography and rigidity layering; Figure 2d), the dike propagated laterally at the interface between the upper and lower layer, stopping below the plain and erupting after 1960 s (~9 days in nature). The final shape was elliptical (*B*/*H* = 2.28), though "inflated" toward the plain, 33.8 cm long. The mean lateral and vertical propagation velocities were 0.24 and 0.17 mm/s, respectively. Moreover, as the dike approached the plain before erupting, it bent toward the *y* axis, reaching an angle $\alpha = 70°$ between the slope direction and the dike strike (Figure S1c in the supporting information).

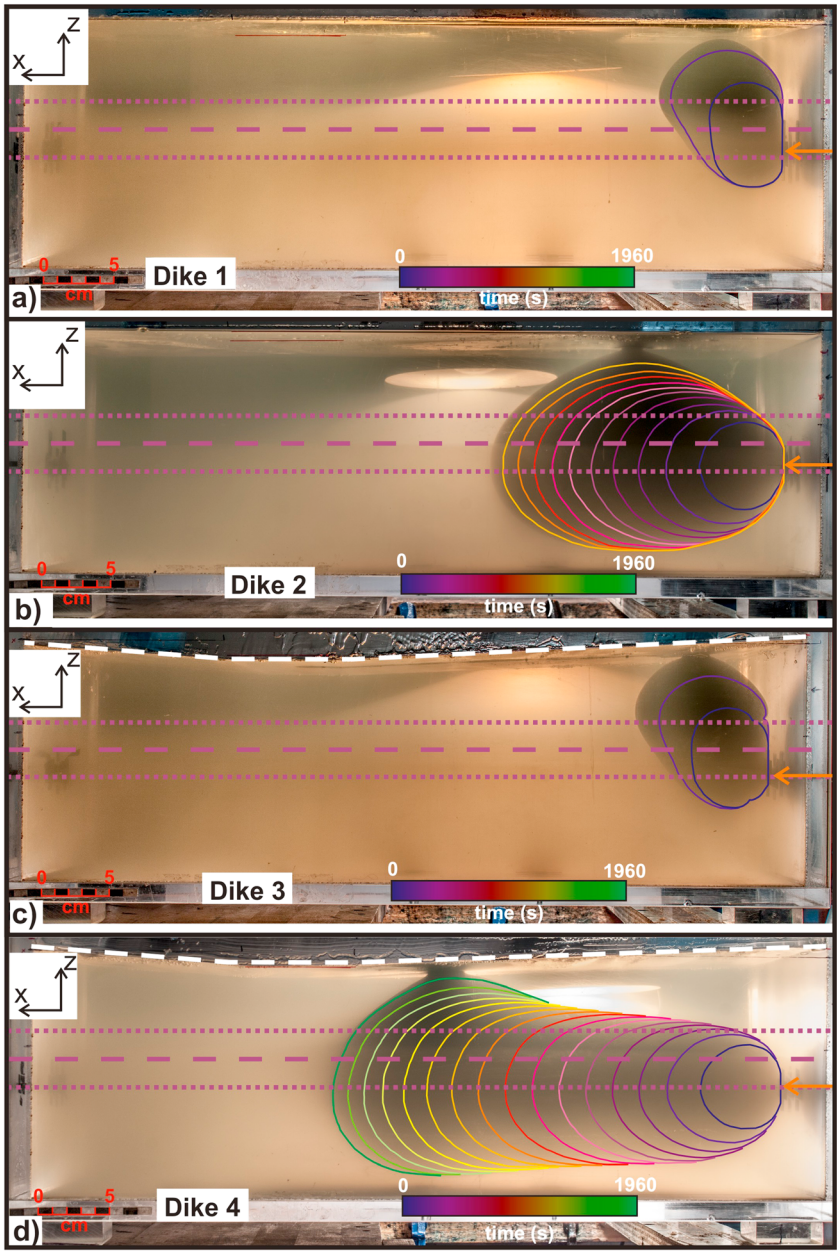

Figure 2. Experiments with flat topography, (a) density (experiment 1) and (b) rigidity layering (experiment 2). Experiments with topography, (c) density (experiment 3) and (d) rigidity layering (experiment 4). The dashed white and purple lines indicate the surface and the center of the interface, respectively. The dotted purple lines indicate the limits of the interface. The orange arrows indicate the injection points. The colored lines indicate the dike edge contour every 120 s.

In experiment 5 (enhanced topography and rigidity layering), we increased the downslope dip (from 2.4° to 7°) and plain (from 0° to 4°), letting the upslope become flat (from 3.7° to 0°; Figures S1a and S1b). The dike, after the injection below the slope on the right (Figure S1a), propagated laterally bending toward the *y* axis, reaching $\alpha = 20°$ (Figure S1b).

We find that rigidity layering, particularly when combined to a slope, leads to longer dikes: higher rigidity ratios, E_u/E_l, result in higher *S*/*T* (Figure 3a) with maximum *S*/*T* (ratio between dike length and injection depth) obtained in experiment 4, with high rigidity contrast and load gradient (Figure 3a). Experiments 1 and 3 (only density layering) have similar *S*/*T* (0.86 and 0.91, respectively), while experiments 2 and 4, with density and rigidity layering, show a much higher *S*/*T* (3.38 and 2.14, respectively). The *S*/*X* ratio appears more uniform,

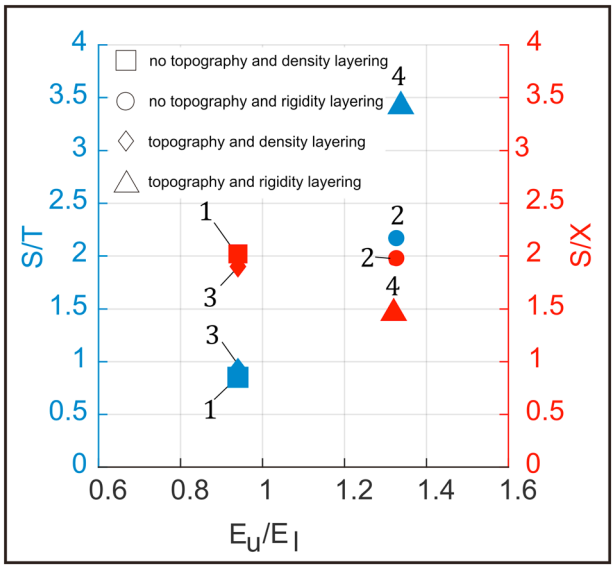

Figure 3. Rigidity ratio (E_u/E_l) against the ratio between dike length and depth of the injection point (*S/T*, blue) and the ratio between dike length and the distance between the injection and eruption points (*S/X*, red).

although experiments 1 and 3 show a smaller difference ($\Delta S/X = 0.12$) with respect to experiments 2 and 4 ($\Delta S/X = 0.47$). Experiments 1 and 3 show low *S/T* values with respect to experiments 2 and 4 (equal to 0.86, 0.91, 2.14, and 3.38, respectively; Figure 3 a), indicating that density layering has minor influence on dike shape.

3.2. Numerical Models

To better understand dike propagation and arrest, we evaluate the stress pattern within the gelatin. We generate a finite element model with COMSOL Multiphysics®. We assume 2-D plane strain, on the *x-z* plane. We set zero displacement both for the lateral and bottom boundaries; the surface, shaped as in the experiments, is stress-free. The properties of the subdomains are density $\rho = 1000$ kg m^{-3}, Young's modulus $E = 3500$ Pa, and Poisson's ratio $\nu = 0.4999$. Gravity mimics the laboratory conditions, so that the stresses include the gelatin load [e.g., *Corbi et al.*, 2016].

The model shows that the minimum compressive stress σ_3 is subhorizontal beneath the slopes and rotates progressively to subvertical beneath the plain (Figure 4a). Such a configuration where σ_3 is lying on the *x-z* plane favors in general dike strikes along the *y* axis (perpendicular to the figure plane), explaining the bending toward the *y* axis observed in experiment 4 (Figure S1c). This effect is enhanced if the slope dip is increased (experiment 5; Figure S1b). The dike in experiment 4 did not reorient, probably because $(\sigma_2 - \sigma_3)/\sigma_2$ was very small, indicating that σ_2 is similar to σ_3 (Figure 4b). Such stress configuration is not particularly affected by the rigidity layering (Figure S2).

Since σ_1 and σ_3 lie on the propagation plane, the stress normal to the dike plane is σ_2, plotted in Figure 4c. The gradient of σ_2 is ~170 Pa m^{-1}. Revising the ratio of buoyancy to loading gradient estimated in equation (7), we obtain 1.1. The lateral gradient in our experiments may be too low to correctly simulate the 2014 Bardarbunga dike. However, we observe that the propagating tip of our dikes becomes arrested where σ_2 is minimum before increasing again (Figure 4c). This observation highlights that a nonzero driving gradient is essential for lateral propagation. Since σ_2 is large below the "mountain" and decreases downslope, it compresses the dike tail and squeezes its front toward the plain, further promoting lateral propagation. Conversely, below the upslope, the increase of σ_2 compresses the dike tip, arresting the dike where σ_2 is minimum (Figure 4c).

4. Discussion and Conclusions

Our models suggest that lateral dike propagation is promoted by several factors: (1) vertical dike ascent needs to be prevented; (2) the dike must be pushed laterally by a pressure gradient; and (3) for highest efficiency, this pressure gradient should be maximum in the direction perpendicular to σ_3. Below we discuss these factors and their relevance for dike propagation in nature, recalling that in our experiments σ_3 was in the plane of the dike. Even though we cannot properly evaluate what would have changed if σ_3 was dike-perpendicular, available evidence from magmatic systems along divergent plate boundaries suggests that this promotes further lateral propagation [*Acocella*, 2014].

Regarding point (1), in experiments 2 and 4 we prevented vertical dike ascent and obtained lateral propagation through rigidity layering. These experiments suggest that rigidity layering is more efficient than

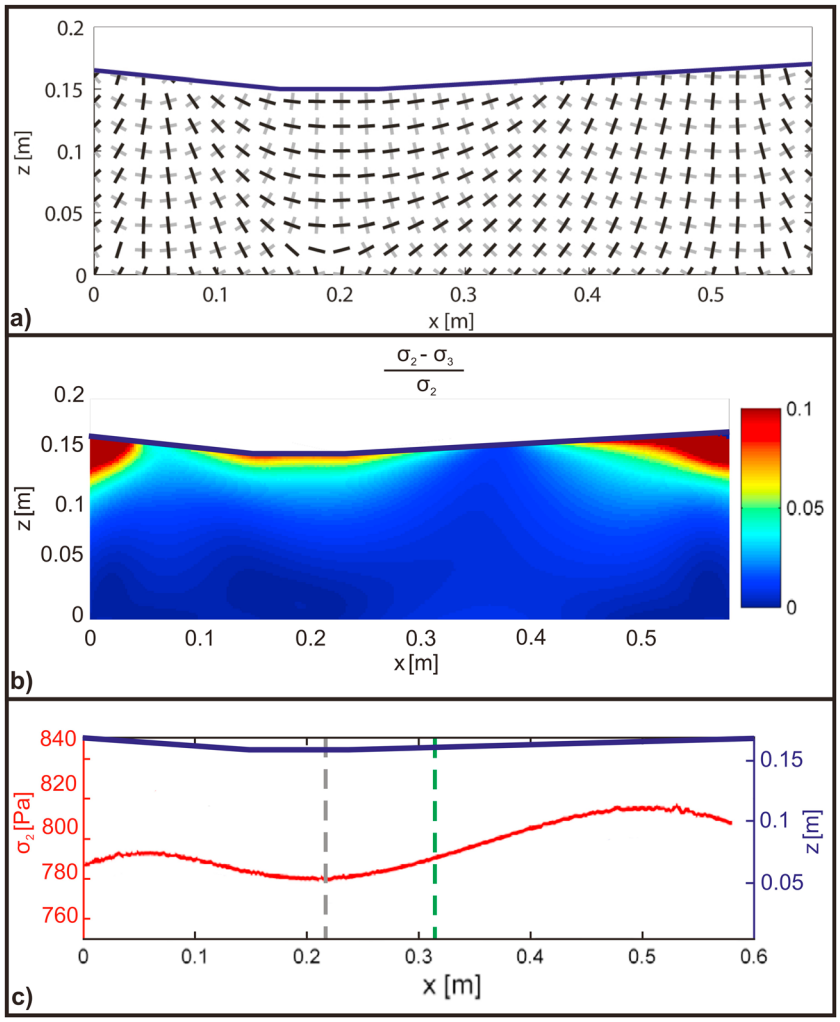

Figure 4. Stresses in the gelatin experiments. (a) Direction of the principal stress components σ1 (black lines) and σ3 (gray lines). (b) The (σ2 − σ3)/σ2 variations due to the imposed topography. (c) The σ2 profile (red line). The blue line indicates the topography profile; the dashed green and gray lines indicate the eruption point and the final position of the dike tip in experiment 4, respectively.

antibuoyancy in driving lateral dike propagation, as it acts as a barrier to ascent, while antibuoyancy determines only the vertical equilibrium position of the dike [*Rivalta et al.*, 2015]. However, models of dike injection at the base of a box with soft layers above stiff ones suggest that vertical propagation is promoted [*Rivalta et al.*, 2005]. In volcanic areas, stiff layers often overlie softer layers, as soft scoria and/or pyroclastic deposits may be capped by kilometer-thick stiffer lava piles, as in central Afar [*Abbate et al.*, 2015]. This decrease in rigidity with depth affecting dike propagation is exemplified by the 2004 eruption at Asama (Japan), where part of the feeder dike propagated laterally below a stiffer zone [*Aoki et al.*, 2009]. Thermal weakening of the upper crust, due to the presence of partial melt or to chemical reactions triggered by heat advection, may also decrease the rigidity of the rock, so that this becomes more compliant at depth [*Heap et al.*, 2013]. These wide-scale rigidity inversions are geophysically detected below rifts, as Kilauea's East Rift Zone (Hawaii), Krafla (Iceland), and Afar [*Brandsdottir et al.*, 1997; *Haslinger et al.*, 2001; *Desissa et al.*, 2013] and, possibly, at Bardarbunga, with the vent located within a basin with alternating sediments and lavas.

Other processes may inhibit vertical dike propagation. Magma may be more antibuoyant in the shallowest layers than what modeled here. Additionally, graben faulting may arrest an ascending dike by compressing its upper tip, as suggested for the 2009 dike at Harrat Lunayyir (Saudi Arabia) [*Xu et al.*, 2016]. These processes may be more important than previously thought for lateral propagation.

As for points (2) and (3), a lateral pressure gradient is necessary to drive dikes to larger distances. We imposed a lateral gradient by shaping the topography of our gelatin similar to a volcanic slope, even though other factors may induce lateral stress gradients. Here we have shown that a lateral pressure gradient is not very efficient in driving dike propagation if σ_3 is not perpendicular to the dike. This was already demonstrated by *Dahm* [2000], who compared with a numerical model dike trajectories for three cases: (a) pressure gradient with $\sigma_1 = \sigma_3$, (b) pressure gradient aligned with σ_3, and (c) pressure gradient perpendicular to σ_3. In case (c), where the two factors (pressure gradient and σ_3) reinforced each other, the dike deviated toward the maximum gradient direction over a short distance. In case (a), a larger distance was needed for the dike to bend and align with the maximum gradient direction. In case (b), where the two factors played against each other, the dike bent toward an intermediate direction.

The pathway of the Bardarbunga dike resulted from a combination of tectonic and loading stresses [*Sigmundsson et al*., 2015]. The final strike of the dike deviated from that perpendicular to the maximum tectonic extension by 10°, as shown by deformation models and focal mechanisms of earthquakes [*Ruch et al*., 2016; *Ágústsdóttir et al*., 2016]. Here we confirm that any inconsistency between the direction of the maximum topographic gradient and that perpendicular to σ_3 leads to dike bending and shearing on the dike plane. In nature, surface loads may have more complex 3-D distributions. Indeed, at stratovolcanoes, σ_3 is horizontal and circumferential around the volcanic cone; thus, as the dike propagates downslope, the bending observed in the experiments would not take place, unless other factors contribute to the stress field, such as preexisting fractures [*Le Corvec et al*., 2013; *Ruch et al*., 2016] or regional tectonics [*Sigmundsson et al*., 2015], both not modeled here.

As for the factors causing dike arrest below the plain in our experiments, we speculate that the lithostatic load of the opposite slope acts as a "pressure barrier," compressing the propagating tip and thus hindering dike propagation, as suggested for Somma-Vesuvio [*Acocella et al*., 2006] or Miyakejima [*Maccaferri et al*., 2016]. This is also supported by the model of the σ_2 profile with single slope compared to that of a double slope (Figure S3): with two opposite slopes σ_2 increases upslope, while with a single slope σ_2 keeps decreasing. Therefore, the dike would propagate farther without any upslope.

An important role may be also played by the stress induced in the gelatin by the specific distribution of loads, which involves a subvertical σ_3 beneath the plain and a subhorizontal σ_3 moving toward the slopes, as in Figure 4a and previous studies [e.g., *Maccaferri et al*., 2014]. This stress pattern causes the experimental dike to bend sideways and stop, as the more it bends the smaller the topographic gradient it experiences.

Our results help interpreting some features of recent lateral diking events (such as Bardarbunga in 2014). In experiment 4, we observe dike arrest in a region of flat and low topography, similar to the southern flank of Askja volcano, encountered by the 2014 Bardarbunga dike on its pathway. We note a discrepancy in the position of the eruption point, which is before the plain in the models and inside the plain in Bardarbunga, and in the final position of the dike tip, which is at ~10 km from the plain edge in Bardarbunga and 3.3 cm (corresponding to ~2 km in nature) in experiment 4. Experiments 15 and 16 (replicating experiment 4, except for the layer thicknesses; Table S1) also erupted before the plain ($X = 15.1$ cm and 20.1 cm, respectively), confirming reproducibility. However, the Bardarbunga dike intersected the surface in three more locations beside the plain (where two major vents opened). In fact, three cauldrons formed on the Vatnajökull ice cap [*Sigmundsson et al*., 2015]. The longest dike in our models (experiment 4 = 33.8 cm corresponding to ~18 km in nature) has the same order of magnitude of the dike segment that propagated laterally under the ice cap at Bardarbunga (~30 km).

Concerning the 2005 Dabbahu diking episode, the southern portion arrested just before a region of minor relief (height difference of 300 m compared to 400 and 300 m for Bardarbunga and Somma-Vesuvio, respectively); conversely, the northern part of the dike propagated upslope erupting on the NE flank of the edifice [*Wright et al*., 2006; *Ebinger et al*., 2010]. In this case, the effect on crustal stresses of a lateral thermal gradient of the crust may have dominated over the effect of topography [*Grandin et al*., 2012] and allowed the dike propagating upslope for some distance, possibly explaining the discrepancy with our models that suggest a difficulty in propagating along an opposite slope. This confirms, as mentioned, that other processes in addition to topography may drive lateral propagation and arrest.

In conclusion, lateral dike propagation downslope is particularly efficient when the topographic pressure gradient is accompanied with crustal rigidity layering (i.e., stiffer layers above weak ones). Conversely, dikes may arrest if an external relief produces an opposite topographic pressure gradient.

Acknowledgments
Giulia Sili provided technical support during the experiments. Matteo Trolese provided useful suggestions for the image processing. Malte C. Ritter shared his data about gelatin rigidity. Janine Kavanagh provided helpful advices for the setting of the analogue models. Laurent Michon provided helpful suggestions. Nicolas Le Corvec, Robert White, and Joel Ruch provided constructive reviews. This work was financed by the Italian government. Any user can access the data of this work by contacting the corresponding author.

References

Abbate, E., P. Bruni, and M. Sagri (2015), Geology of Ethiopia: A review and geomorphological perspectives, in *Landscapes and Landforms of Ethiopia, World Geomorphological Landscapes*, edited by P. Billi, pp. 33–64, Springer, Dordrecht, Netherlands, doi:10.1007/978-94-017-8026-1_2.

Acocella, V. (2014), Structural control on magmatism along divergent and convergent plate boundaries: Overview, model, problems, *Earth Sci. Rev.*, *136*, 226–288, doi:10.1016/j.earscirev.2014.05.006.

Acocella, V., and A. Tibaldi (2005), Dike propagation driven by volcano collapse: A general model tested at Stromboli, Italy, *Geophys. Res. Lett.*, *32*, L08308, doi:10.1029/2004GL022248.

Acocella, V., M. Porreca, M. Neri, E. Massimi, and M. Mattei (2006), Propagation of dikes at Vesuvio (Italy) and the effect of Mt. Somma, *Geophys. Res. Lett.*, *33*, L08301, doi:10.1029/2005GL025590.

Ágústsdóttir, T., J. Woods, T. Greenfield, R. G. Green, R. S. White, T. Winder, B. Brandsdóttir, S. Steinthórsson, and H. Soosalu (2016), Strike-slip faulting during the 2014 Bárðarbunga-Holuhraun dike intrusion, central Iceland, *Geophys. Res. Lett.*, *43*, 1495–1503, doi:10.1002/2015GL067423.

Aoki, Y., et al. (2009), *P*-wave velocity structure beneath Asama Volcano, Japan, inferred from active source seismic experiment, *J. Volcanol. Geotherm. Res.*, *187*, 272–277, doi:10.1016/j.jvolgeores.2009.09.004.

Brandsdottir, B., W. Menke, P. Einarsson, R. S. White, and R. K. Staples (1997), Faroe-Iceland ridge experiment: 2. Crustal structure of the Krafla central volcano, *J. Geophys. Res.*, *102*, 7867–7886, doi:10.1029/96JB03799.

Brizzi, S., F. Funiciello, F. Corbi, E. Di Giuseppe, and G. Mojoli (2016), Salt matters: How salt affects the rheological and physical properties of gelatine for analogue modelling, *Tectonophysics*, *679*, 88–101, doi:10.1016/j.tecto.2016.04.021.

Buck, W. R., P. Einarsson, and B. Brandsdóttir (2006), Tectonic stress and magma chamber size as controls on dike propagation: Constraints from the 1975–1984 Krafla rifting episode, *J. Geophys. Res.*, *111*, B12404, doi:10.1029/2005JB003879.

Corbi, F., E. Rivalta, V. Pinel, F. Maccaferri, M. Bagnardi, and V. Acocella (2015), How caldera collapse shapes the shallow emplacement and transfer of magma in active volcanoes, *Earth Planet. Sci. Lett.*, *431*, 287–293, doi:10.1016/j.epsl.2015.09.028.

Corbi, F., E. Rivalta, V. Pinel, F. Maccaferri, and V. Acocella (2016), Understanding the link between circumferential dikes and eruptive fissures around calderas based on numerical and analog models, *Geophys. Res. Lett.*, *43*, 6212–6219, doi:10.1002/2016GL068721.

Dahm, T. (2000), Numerical simulations of the propagation path and arrest of fluid-filled fractures in the Earth, *Geophys. J. Int.*, *141*, 623–638, doi:10.1046/j.1365-246x.2000.00102.x.

Dahm, T., S. Hainzl, and T. Fischer (2010), Bidirectional and unidirectional fracture growth during hydrofracturing: Role of driving stress gradients, *J. Geophys. Res.*, *115*, B12322, doi:10.1029/2009JB006817.

Desissa, M., N. E. Johnson, K. A. Whaler, S. Hautot, S. Fisseha, and G. J. K. Dawes (2013), A mantle magma reservoir beneath an incipient mid-ocean ridge in Afar, Ethiopia, *Nat. Geosci.*, *6*(10), 861–865, doi:10.1038/ngeo1925.

Di Giuseppe, E., F. Funiciello, F. Corbi, G. Ranalli, and G. Mojoli (2009), Gelatins as rock analogs: A systematic study of their rheological and physical properties, *Tectonophysics*, *473(3–4)*, 391–403, doi:10.1016/j.tecto.2009.03.012.

Ebinger, C. J., A. Ayele, D. Keir, J. Rowland, G. Yirgu, T. Wright, M. Belachew, and I. Hamling (2010), Length and timescales of rift faulting and magma intrusion: The Afar rifting cycle from 2005 to present, *Annu. Rev. Earth Planet. Sci.*, *38(1)*, 439–466, doi:10.1146/annurev-earth-040809-152333.

Fialko, Y. A., and A. M. Rubin (1999), What controls the along-strike slopes of volcanic rift zones?, *J. Geophys. Res.*, *104(B9)*, 20,007–20,020, doi:10.1029/1999JB900143.

Fiske, R. S., and E. D. Jackson (1972), Orientation and growth of Hawaiian volcanic rifts: The effect of regional structure and gravitational stresses, *Proc. R. Soc. Lond. A*, *329*, 299–326, doi:10.1098/rspa.1972.0115.

Grandin, R., A. Socquet, C. Doubre, E. Jacques, and G. C. P. King (2012), Elastic thickness control of lateral dyke intrusion at mid-ocean ridges, *Earth Planet. Sci. Lett.*, *319–320*, 83–95, doi:10.1016/j.epsl.2011.12.011.

Gudmundsson, A. (2002), Emplacement and arrest of sheets and dykes in central volcanoes, *J. Volcanol. Geotherm. Res.*, *116*, 279–298, doi:10.1016/S0377-0273(02)00226-3.

Gudmundsson, A. (2003), Surface stresses associated with arrested dykes in rift zones, *Bull. Volcanol.*, *65*, 606–619, doi:10.1007/s00445-003-0289-7.

Gudmundsson, A. (2011), Deflection of dykes into sills at discontinuities and magma-chamber formation, *Tectonophysics*, *500(1–4)*, 50–64, doi:10.1016/j.tecto.2009.10.015.

Gudmundsson, M. T., et al. (2016), Gradual caldera collapse at Bárdarbunga volcano, Iceland, regulated by lateral magma outflow, *Science*, *353*, aaf8988, doi:10.1126/science.aaf8988.

Haslinger, F., C. Thurber, M. Mandernach, and P. Okubo (2001), Tomographic image of *P*-velocity structure beneath Kilauea's East Rift Zone and south flank: Seismic evidence for a deep magma body, *Geophys. Res. Lett.*, *28(2)*, 375–378, doi:10.1029/2000GL012018.

Heap, M. J., S. Mollo, S. Vinciguerra, Y. Lavallée, K.-U. Hess, D. B. Dingwell, P. Baud, and G. Iezzi (2013), Thermal weakening of the carbonate basement under Mt. Etna volcano (Italy): Implications for volcano instability, *J. Volcanol. Geotherm. Res.*, *250*, 42–60, doi:10.1016/j.jvolgeores.2012.10.004.

Kavanagh, J. L., T. Menand, and R. S. J. Sparks (2006), An experimental investigation of sill formation and propagation in layered elastic media, *Earth Planet. Sci. Lett.*, *245*, 799–813, doi:10.1016/j.epsl.2006.03.025.

Kavanagh, J. L., T. Menand, and K. A. Daniels (2013), Gelatine as a crustal analogue: Determining elastic properties for modelling magmatic intrusions, *Tectonophysics*, *582*, 101–111, doi:10.1016/j.tecto.2012.09.032.

Kervyn, M., G. G. J. Ernst, B. V. W. De Vries, L. Mathieu, and P. Jacobs (2009), Volcano load control on dyke propagation and vent distribution: Insights from analogue modeling, *J. Geophys. Res.*, *114*, B03401, doi:10.1029/2008JB005653.

Le Corvec, N., T. Menand, and J. Lindsay (2013), Interaction of ascending magma with pre-existing crustal fractures in monogenetic basaltic volcanism: An experimental approach, *J. Geophys. Res. Solid Earth*, *118*, 968–984, doi:10.1002/jgrb.50142.

Lister, J. R. (1990), Buoyancy-driven fluid fracture: Similarity solutions for the horizontal and vertical propagation of fluid-filled cracks, *J. Fluid Mech.*, *217*, 213–239, doi:10.1017/S0022112090000696.

Lister, J. R. (1991), Steady solutions for feeder dykes in a density-stratified lithosphere, *Earth Planet. Sci. Lett.*, *107*, 233–242, doi:10.1016/0012-821X(91)90073-Q.

Lister, J. R., and R. C. Kerr (1991), Fluid-mechanical models of crack propagation and their application to magma transport in dykes, *J. Geophys. Res.*, *96*(B6), 1049–1077, doi:10.1029/91JB00600.

Maccaferri, F., M. Bonafede, and E. Rivalta (2011), A quantitative study of the mechanisms governing dike propagation, dike arrest and sill formation, *J. Volcanol. Geotherm. Res.*, *208*(1–2), 39–50, doi:10.1016/j.jvolgeores.2011.09.001.

Maccaferri, F., E. Rivalta, D. Keir, and V. Acocella (2014), Off-rift volcanism in rift zones determined by crustal unloading, *Nat. Geosci.*, *7*, 297–300, doi:10.1038/NGEO2110.

Maccaferri, F., E. Rivalta, L. Passarelli, and Y. Aoki (2016), On the mechanisms governing dike arrest: Insight from the 2000 Miyakejima dike injection, *Earth Planet. Sci. Lett.*, *434*, 64–74, doi:10.1016/j.epsl.2015.11.024.

Olson, J. E., and R. A. Schultz (2011), Comment on "A note on the scaling relations for opening mode fractures in rock" by C.H. Scholz, *J. Struct. Geol.*, *33*(10), 1523–1524, doi:10.1016/j.jsg.2011.07.004.

Pinel, V., and C. Jaupart (2000), The effect of edifice load on magma ascent beneath a volcano, *Phil. Trans. R. Soc. Lond. A*, *358*, 1515–1532, doi:10.1098/rsta.2000.0601.

Pinel, V., and C. Jaupart (2004), Magma storage and horizontal dyke injection beneath a volcanic edifice, *Earth Planet. Sci. Lett.*, *221*, 245–262, doi:10.1016/S0012-821X(04)00076-7.

Pinel, V., and C. Jaupart (2005), Some consequences of volcanic edifice destruction for eruption conditions, *J. Volcanol. Geotherm. Res.*, *145*, 68–80, doi:10.1016/j.jvolgeores.2005.01.012.

Ritter, M. C. (2012), Analogue and numerical modelling of dyke propagation in stratovolcanoes effects of rock mechanical properties and layer thicknesses, M.S. thesis, Dep. of Struct. Geol. and Geodynamics, Univ. of Göttingen, Göttingen, Germany.

Ritter, M. C., V. Acocella, J. Ruch, and S. L. Philipp (2013), Conditions and threshold for magma transfer in the layered upper crust: Insights from experimental models, *Geophys. Res. Lett.*, *40*, 1–5, doi:10.1002/2013GL058199.

Rivalta, E., M. Bottinger, and T. Dahm (2005), Buoyancy-driven fracture ascent: Experiments in layered gelatine, *J. Volcanol. Geotherm. Res.*, *144*, 273–285, doi:10.1016/j.jvolgeores.2004.11.030.

Rivalta, E., B. Taisne, A. P. Bunger, and R. F. Katz (2015), A review of mechanical models of dike propagation: Schools of thought, results and future directions, *Tectonophysics*, *638*, 1–42, doi:10.1016/j.tecto.2014.10.003.

Roman, A., and C. Jaupart (2014), The impact of a volcanic edifice on intrusive and eruptive activity, *Earth Planet. Sci. Lett.*, *408*, 1–8, doi:10.1016/j.epsl.2014.09.016.

Rubin, A. M. (1995), Propagation of magma-filled cracks, *Annu. Rev. Earth Planet. Sci.*, *23*(1), 439–466, 287–336, doi:10.1146/annurev.ea.23.050195.001443.

Ruch, J., T. Wang, W. Xu, M. Hensch, and S. Jonsson (2016), Oblique rift opening revealed by reoccurring magma injection in central Iceland, *Nat. Commun.*, *7*, 1–7, doi:10.1038/ncomms12352.

Ryan, M. P. (1994), Neutral-buoyancy controlled magma transport and storage in mid-ocean ridge magma reservoirs and their sheeted-dike complex: A summary of basic relationships, in *Magmatic Systems*, edited by M. P. Ryan, pp. 97–135, Academic Press, San Diego, Calif.

Scholz, C. H. (2010), A note on the scaling relations for opening mode fractures in rock, *J. Struct. Geol.*, *32*(10), 1485–1487, doi:10.1016/j.jsg.2010.09.007.

Sigmundsson, F., et al. (2015), Segmented lateral dyke growth in a rifting event at Bárðarbunga volcanic system, Iceland, *Nature*, *517*, 191–195, doi:10.1038/nature14111.

Taisne, B., and C. Jaupart (2009), Dike propagation through layered rocks, *J. Geophys. Res.*, *114*, B09203, doi:10.1029/2008JB006228.

Turcotte, D. L., and G. Schubert (2002), *Geodynamics*, 435 pp., Cambridge Univ. Press, Cambridge, England.

Watanabe, T., T. Masuyama, K. Nagaoka, and T. Tahara (2002), Analog experiments on magma-filled cracks: Competition between external stresses and internal pressure, *Earth Planets Space*, *54*, 1247–1261, doi:10.1186/BF03352453.

Wright, T. J., C. Ebinger, J. Biggs, A. Ayele, G. Yirgu, D. Keir, and A. Stork (2006), Magma-maintained rift segmentation at continental rupture in the 2005 Afar dyking episode, *Nature*, *442*, 291–294, doi:10.1038/nature04978.

Wright, T. J., et al. (2012), Geophysical constraints on the dynamics of spreading centres from rifting episodes on land, *Nat. Geosci.*, *5*(4), 242–250, doi:10.1038/ngeo1428.

Xu, W., S. Jónsson, F. Corbi, and E. Rivalta (2016), Graben formation and dike arrest during the 2009 Harrat Lunayyir dike intrusion in Saudi Arabia: Insights from InSAR, stress calculations and analog experiments, *J. Geophys. Res. Solid Earth*, *121*, 2837–2851, doi:10.1002/2015JB012505.